Structural behaviour of GFRP beams subjected to concentrated loads: experimental tests, numerical modeling and analytical study

Lourenço Almeida Fernandes, IST/DE Civil

Abstract: GFRP composites have shown an increased growth in civil engineering applications; however, this growth has been hindered by the absence of mature legal documents. This dissertation fits this framework, adding research and data to the understanding of this material; in particular, the research focuses on the web-crippling phenomenon in GFRP I-shaped pultruded beams, due to concentrated loads. The research can be divided into three different levels: (i) the experimental research, (ii) the numerical simulation and (iii) the analytical research. The experimental work can be split into two levels: the mechanical characterization of the material and the experimental research on web-crippling. The first level is crucial for the correct calibration of numerical models and design equations, while the second is aligned with the main objective of this dissertation. The numerical study consisted in the simulation of the web-crippling tests, in order to study possible buckling behavior, stress distributions and failure criteria. The analytical study consisted of gathering different design formulae, concerning web-crippling and web-buckling failure. This process began with the gathering of formulas designed for GFRP beams and was extended to steel design formulas. After assessing the efficacy of the various design equations, a new empirical expression was developed.

Keywords: GFRP pultruded profiles, concentrated loads, web-crippling, experimental tests; numerical simulation, analytical investigation.

1 - Introduction

The study of web-crippling phenomena in GFRP beams is still in the first stages of development. The research described here aims at improving the knowledge on this matter and is framed in a broader research project in course at *Instituto Superior Técnico* (IST) [1-6]. This framework allowed for synergies to take place, expediting experimental procedures and preventing mistakes already detected and corrected. In particular, the research conducted by Correia [4] and Nunes *et al.* [5, 6] contributed directly to the current study, namely the mechanical characterization tests developed by these authors.

Borowicz and Bank [7-9] have led the main and pioneering efforts in studying web-crippling in GFRP beams. However, their research has focused on a single experimental configuration, Interior One Flange (IOF). The four main configurations in the literature are End One Flange (EOF), IOF, End Two Flange (ETF) and Interior Two Flange (ITF); the first two configurations are based on a three-point-bending setup, with the rupture occurring at the end (EOF) or interior (IOF) sections; on the other hand, the ETF and ITF configurations consist of the transversal loading of both flanges, in a single section, either interior (ITF) or at the extremity of the beam (ETF). The research described here was solely focused on the latter configurations, ETF and ITF, as they were not properly addressed until now. However, it is worth mentioning the work related to these two configurations performed by Wu and Bai [10] on square hollow sections. These authors also took into account experimental configurations where the test specimens are fully supported on the bottom flange.

In the present paper, four different GFRP I-shaped profiles were studied. The various profiles present unique properties and geometries amongst them, having been supplied by two different producers. The test specimens were tested with steel bearing plates, presenting three different bearing lengths. This variety contributes towards the goal of undertaking a comprehensive study about the web-crippling phenomenon. The experimental research was complemented by a numerical simulation, which allowed for a deeper study, in terms of stress distributions and buckling phenomena. The numerical simulation also took into account the Tsai-Hill criterion in order to compare experimental and numerical failure loads. Finally, the main design formulae for web-crippling and web-buckling failure, designed for GFRP beams, were gathered and compared to the

experimental results, showing poor efficacy. The poor matching between design and experimental values motivated the development of an empirical design formula, based on design equations developed for steel structures.

2 - Experimental Program

2.1 - Test Specimens

The experimental research focused on four different I-shaped profiles, with heights of 100, 120, 200 and 400 mm. The geometry of the various sections is presented in Table 1.
All tested profiles presented length-to-depth ratios of 2. The I120 beam was provided by *Fiberline Composites*, while the remaining three profiles were supplied by *Alto Perfis Pultrudidos*. The difference in supplier may be very relevant in an FRP element, since small changes in the pultrusion process and in the laminate composition may cause significant variations in a beam's/column's behavior.

Table 1: Geometry of the test specimens.

Profile	Suppl.	Depth (mm)	Flange width (mm)	Web thickness (mm)
I100	Alto	100	50	8
I120	Fiber.	120	60	6
I200	Alto	200	100	10
I400	Alto	400	200	15

The mechanical characterization campaign is crucial for both the correct development of numerical models and the correct calibration of design formulae. This experimental campaign focused solely on the I100 and I400 beams, as both the I120 and the I200 had already been analyzed in previous campaigns by Nunes *et al.* [6] and Correia [4]. The properties obtained in this experimental campaign are presented in Table 2, alongside the properties gathered in those previous studies. The values presented in Table 2 only refer to web properties (in the longitudinal (L) and transverse (T) directions).
In the experimental study on web-crippling, three bearing lengths were considered: 15, 50 and 100 mm, except for the I400 profile, which was only tested for the bearing length of 100 mm (due to material restrictions). Three specimens were tested for each experimental series, in terms of configuration and bearing length. The test specimens were named as follows: the GFRP beam; the experimental configuration (ETF or ITF); the bearing length; and the number of each specimen (numbered 1 to 3 for each series). For example, a specimen obtained from an I120 profile, being the second of the series, tested in the ITF configuration and loaded by a 50 mm long bearing plate is named as follows: I120-ITF-50-2.

2.2 - Experimental Setup and Procedure

The crushing experimental research was conducted in an *Instron* universal testing machine with a load capacity of 250 kN. The bearing plates were welded to the machine base plates, ensuring that both bearing plates were aligned, thus guaranteeing that the load would be applied in the same section of the GFRP beam. The load was applied through displacement control, at an average speed of 0,01 mm/s. Data was acquired with a data logger from *HBM* model *Spider 8* and recorded in *Microsoft Excel* files. Some tests were conducted with a spherical hinge, welded to the bottom flange's bearing plate; however, this support system was too unstable and therefore discarded in subsequent tests. No spherical hinges or cylindrical roller supports were considered in the tests presented in this paper (further information on the tests with spherical hinges is reported in [11]).
Each specimen was loaded until failure, which comprised a sudden loss of applied load. Some specimens were further loaded in order to better identify the failure mechanisms. Finally, all specimens were photographed before and after being tested.

2.3 - Experimental Results and Discussion

2.3.1 - Failure Modes

In the various tests that were conducted, in both the ETF and ITF configurations, two main failure modes were documented: web-crippling and web-buckling. The first failure mode can be separated into two others,

Table 2: Main properties of the GFRP beams under study in the longitudinal (L) and transverse (T) directions (E^t, E^c and E^f – elasticity moduli in tension, compression and bending; G – shear modulus; σ_u^t, σ_u^c and σ_u^f – axial strength in tension, compression and bending; τ_u – in-plane shear strength; f_s – interlaminar shear strength).

Property	I100		I120 [6]		I200 [4]		I400	
	L	T	L	T	L	T	L	T
E^t (GPa)	18,5	-	28.9	-	33,1	-	27,9	4,0
E^c (GPa)	14,0	4,5	28,9	8.5	27,1	5,7	12,2	5,5
σ_u^t (MPa)	426,2	-	308,6	-	375,4	-	296,0	28,4
σ_u^c (MPa)	271,9	73,2	360,3	121,0	434,4	92,6	204,7	70,4
G (GPa)	4,1*		3.9		3,7		3,8	
τ_u (MPa)	19,9*		30,8		24,4		21,0	
E^{fl} (GPa)	23,9		-		24,0		-	
σ_u^{fl} (MPa)	477,8		-		500,8		-	
f_s (MPa)	33,3		-		29,4		-	

*Insufficient number of tests for corroboration.

corresponding to failure occurring near the web-flange junction and in the center of the web; however, these failure modes presented similar cracking configurations. The various failure modes are depicted in Figs. 1 to 4.

The web-crippling failure comprised horizontal cracking along the web-flange junction (Fig. 1) or the center of the web (Fig. 2), and sometimes presented a curved development in the area between both bearing plates (Fig. 3). The web-buckling failure mode was easily distinguishable due to the arched shape of the web (Fig. 4). However, some specimens were identified as presenting a web-buckling failure with minimum arch behavior, in these cases small longitudinal cracks appeared in the center of the web (their failure modes were confirmed through numerical simulation).

One of the main findings in terms of failure modes is that the probability of web-buckling failure occurrence increases with the bearing length. In fact, no test specimens subjected to the smallest bearing plate (15 mm) presented a web-buckling failure. On the other hand, subjects tested in the ETF configuration buckled more easily (for smaller bearing lengths) than corresponding specimens tested in the ITF configuration (the detailed list of failure modes is presented in [11]).

2.3.2 - Strength and Stiffness

As an example, Figs. 5 and 6 present typical vertical load vs. vertical deflection (shortening) curves, obtained in the experimental campaign.

The results presented in Figs. 5 and 6 attest the relevance of the bearing length. It is also important to notice that the increase of the bearing length promotes a more linear behavior in the load-displacement curve.

Fig. 1: Test specimen I200-ETF-15-2: Rupture near the web-flange junction.

Fig. 2: Test specimen I100-ITF-100-1: Rupture in the center of the web.

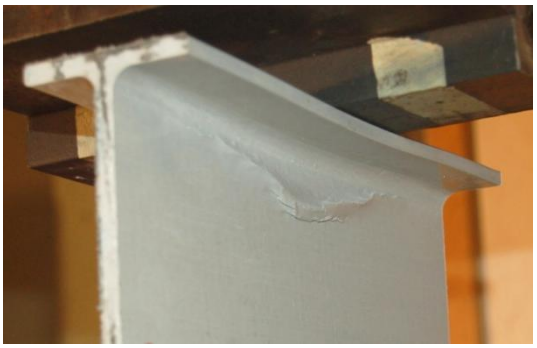

Fig. 3: Test specimen I120-ITF-50-2: Rupture near the web-flange junction (curved cracking).

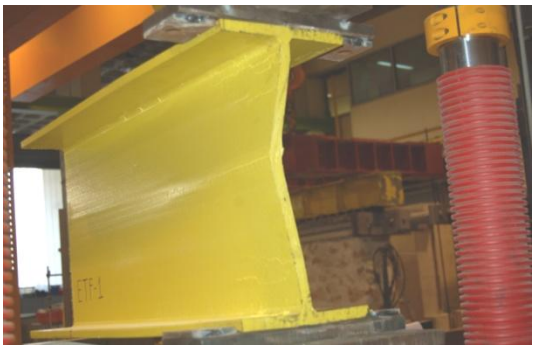

Fig. 4: Test specimen I400-ETF-100-1: Buckling of the web.

The reason for this difference in behavior is the local crushing of the web under the bearing plates, which is more significant when the bearing length is reduced. This trend was noticed in all the beams that were tested for all three bearing plate lengths [11].

The experimental results show that the bearing length can have a great influence on both the resistance and the stiffness (slope of the vertical load vs. vertical deflection curves) of a GFRP beam subjected to a transverse load, in both the ETF and ITF configurations. The results obtained for all GFRP profiles are summarized in Table 3, showing the effect of different bearing lengths on the various test specimens. Table 3 presents average values and the correspondent coefficient of variation (CV).

The change of the bearing length from 15 to 100 mm causes an increase in resistance ranging between 171 and 230% in the ETF configuration, and between 90 and 139% in the ITF configuration. Furthermore, the bearing length also affects the stiffness of the test specimens: a variation from 15 to 100 mm causes an average stiffness increase ranging from 193 and 223% in the ETF configuration, and from 86 and 129% in the ITF configuration.

3 - Numerical Simulation

3.1 - Model Description

The numerical simulation of the tests was developed within the framework of finite element code *Abaqus* [12]. The models were developed by means of written input files, later analyzed in the graphical interface of the program. The numerical models developed

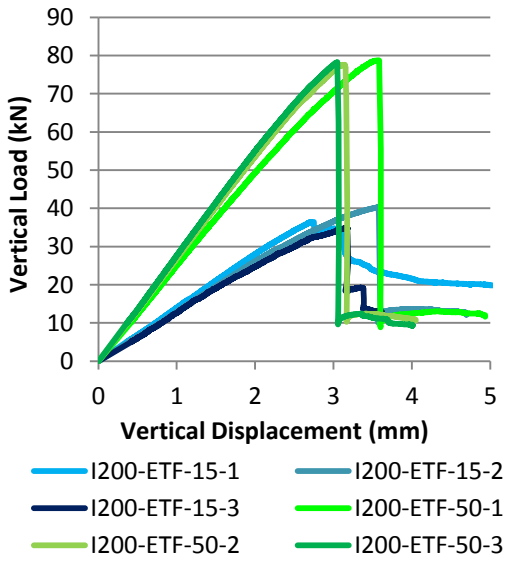

Fig. 5: Results for the test series I200-ETF-15 and I200-ETF-50.

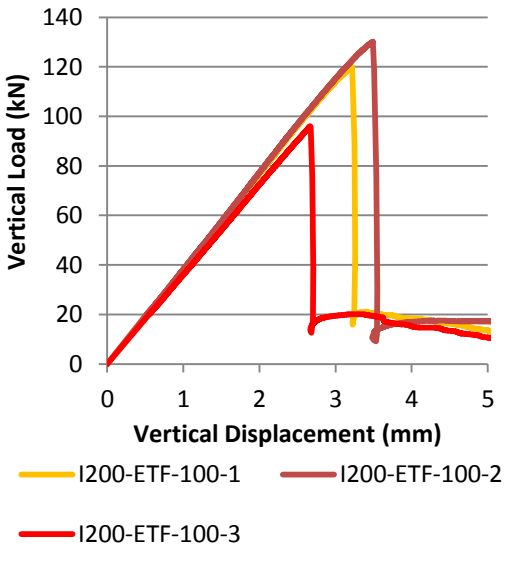

Fig. 6: Results for the test series I200-ETF-100.

Table 3: Average results for the crushing tests.

Beam	Bearing Length (mm)	ETF				ITF			
		Resistance (kN)		Stiffness (kN/mm)		Resistance (kN)		Stiffness (kN/mm)	
		Average	CV	Average	CV	Average	CV	Average	CV
I100	15	16,8	19,0%	12,2	22,4%	29,8	5,6%	18,1	2,4%
	50	38,2	22,5%	27,0	20,2%	41,1	7,6%	29,4	1,9%
	100	45,5	8,2%	36,0	0,3%	56,5	12,2%	40,1	7,7%
I120	15	19,7	1,0%	13,2	1,7%	32,2	3,8%	20,1	0,2%
	50	38,9	7,3%	26,7	1,5%	52,0	3,5%	32,2	0,5%
	100	64,9	6,1%	42,6	0,9%	77,0	7,4%	46,1	0,3%
I200	15	37,2	7,6%	12,9	7,7%	67,8	5,6%	23,6	9,0%
	50	78,2	0,8%	26,1	6,3%	109,1	3,4%	33,8	7,2%
	100	115,3	15,2%	37,8	3,5%	161,3	1,1%	44,0	2,3%
I400	100	74,0	12,3%	23,5	4,8%	127,3	5,5%	39,7	7,7%

were based on S4R shell elements. The load was applied through rigid bearing plates, with R3D4 elements. The modeling of the bearing plates required the separation of the model into different "Instances". And it also was necessary to define the contact between the beam and the rigid bearing plates.

Two different model types were defined for each experimental series: (i) the MSI (models without any imperfection); and the MCI (models that include a geometrical imperfection). The MCI were proposed to study the web-buckling failure. Preliminarily, stability analyses were performed to determine the shape of the critical (first buckling) mode and the critical buckling load value. The imperfection has the shape of the critical mode. These models were important to assess their suitability in comparison with the experimental results. This task was done by comparing experimental ultimate loads and critical loads, validated through the failure modes documented in the experimental campaign. Most likely, tested specimens that exhibit buckling failure should present numerical critical loads similar to the ultimate experimental loads.

3.2 - Results and discussion

The results presented in this paper focused on (i) the comparison between experimental and numerical results (in terms of stiffness and critical loads), (ii) the analysis of stress distributions, and (iii) the comparison between experimental and numerical estimation of failure, through the Tsai-Hill criterion. This paper only presents the main results. For a more detailed study, the reader is referred to [11].

3.2.1 - Comparison of numerical and experimental results

The validation of numerical models was achieved through comparisons between numerical and experimental results, in terms of (i) stiffness (test specimens vs. numerical models) and (ii) critical loads and failure modes. Most models showed good suitability regarding the experimental results, both in terms of stiffness and critical loads. With one exception, the I200 profile showed poor efficacy in terms of critical loads: the I200-ETF-50, the I200-ETF-100 and the I200-ITF-100 models presented critical load values lower than the experimental failure loads, while the test specimens showed no indication of buckling phenomena. The comparison between numerical and experimental results is presented in Figs. 7 and 8, referring to the I120-ITF-15 and the I400-ETF-100 series. In these figures both the MSI and the MCI results are presented (the

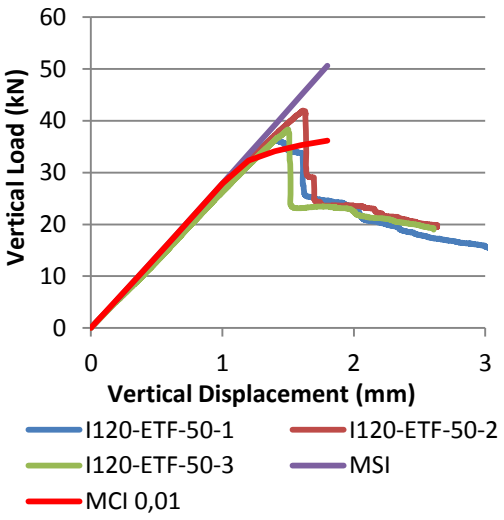

Fig. 7: Comparison between experimental and numerical results for I120-ETF-50.

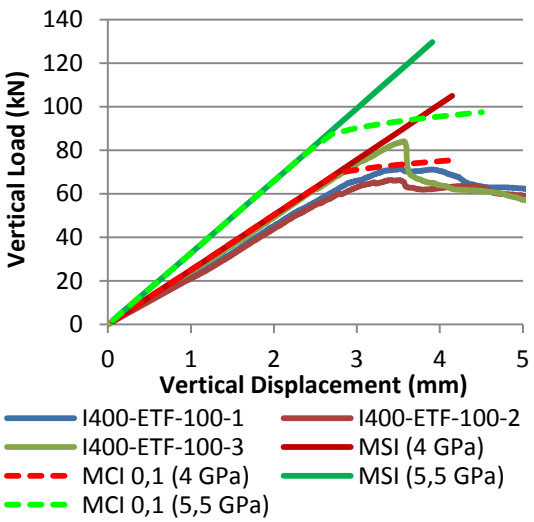

Fig. 8: Comparison between experimental and numerical results for I400-ETF-100.

MCI are presented with the geometric imperfection amplitude in millimeters).

The results presented in Fig. 8 were significant in deciding which elastic modulus value to consider in the transverse direction of the web for the I400 beam. As shown in Table 2, the tensile and compressive results for this parameter were considerably different. The numerical simulation shows great suitability, when considering the tensile elastic modulus. This result leads to the conclusion that it is very important, in the future, to develop an experimental method that can establish the compressive elastic modulus with greater precision. The results of the remaining models can be analyzed in detail in [11].

3.2.2 - Tsai-Hill criterion

The Tsai-Hill criterion is a first failure criterion suited for orthotropic materials such as GFRP, which is given by

$$I_f = \left(\frac{\sigma_1}{\sigma_{1u}}\right)^2 + \left(\frac{\sigma_2}{\sigma_{2u}}\right)^2 - \frac{\sigma_1\sigma_2}{\sigma_{1u}^2} + \left(\frac{\tau_{12}}{\tau_{12u}}\right)^2 \leq 1 \qquad (1)$$

where: σ_1 – acting longitudinal stress; σ_2 – acting transverse stress; τ_{12} – acting shear stress; σ_{1u} – ultimate longitudinal stress; σ_{2u} – ultimate transverse stress; τ_{12u} – ultimate shear stress; I_f – Tsai-Hill failure index. This criterion was employed in order to determine the first failure loads in numerical simulation. However, it must be pointed out that this criterion indicates the failure of a single node (the first to fail) but does not influence the degradation of stiffness due to that node's failure. Since beam collapse is achieved with the failure of many nodes, the Tsai-Hill criterion always gives a conservative estimate of the experimental failure load, and is designated here as initial failure load. The failure loads, provided by this criterion, as well as the ratios between initial failure loads and experimental failure loads, are presented in Table 4. These results clearly indicate that the Tsai-Hill criterion is excessively conservative, when applied to these loading conditions.

3.2.3 - Stress distribution

The numerical simulation also enabled the possibility of studying stress distributions and plots of Tsai-Hill failure index I_f. The stress distribution for the main stress components (transverse and shear stress) and the Tsai-Hill distribution for the I100-ITF-15 MSI are presented in Figs. 9-11. The numerical simulation showed that failure begins near the interior edge of each bearing plate (both edges, in the ITF configuration). When web-buckling occurs, transverse stresses concentrate in the web central zone, causing the failure of the pultruded element. It was also interesting to verify that the Tsai-Hill

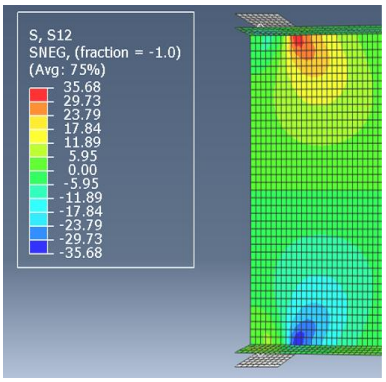

Fig. 9: Shear stress (S12) distribution (16,2 kN).

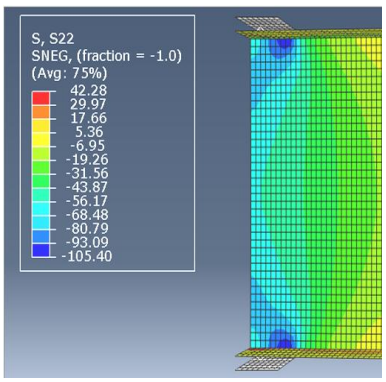

Fig. 10: Transverse stress (S22) distribution (16,2 kN).

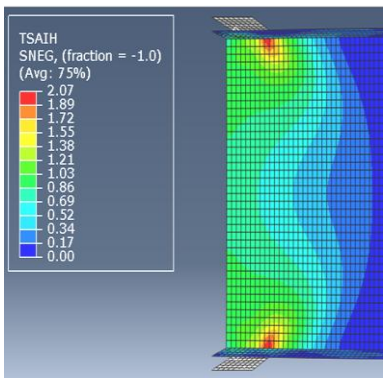

Fig. 11: Tsai-Hill criterion distribution (16,2 kN).

Table 4: Initial failure loads, considering the Tsai-Hill criterion.

Profile	Bearing length (mm)	ETF		ITF	
		Initial failure load (kN)	Initial failure/Experimental failure load Ratio (-)	Initial failure load (kN)	Initial failure/Experimental failure load Ratio (-)
I100	15	7,84	0,47	12,10	0,41
	50	16,20	0,42	20,28	0,49
	100	31,66	0,70	33,73	0,60
I120	15	8,47	0,43	12,77	0,40
	50	17,47	0,45	22,08	0,42
	100	32,81	0,51	37,22	0,48
I200	15	13,86	0,37	23,49	0,35
	50	23,13	0,3	34,7	0,32
	100	38,55	0,33	49,39	0,31
I400	100	47,12	0,66	63,29	0,50

criterion was achieved (I_f=1), in every model, due to the shear stress concentration, near the web-flange junction.

4 - Analytical Study

4.1 - GFRP design formulas

There is still very little research regarding web-crippling of GFRP beams. However, some first-generation design formulas already exist in European and North American codes for GFRP elements. In Europe there are two main references: The Eurocomp Design Code and Handbook [13] and the Italian code [14]. In North America, a pre-standard [15] was published in the scope of Load and Resistance Factor Design (LFRD). In his book [16], Bank also summarized a lot of information about GFRP elements, and presented formulae concerning web-crippling.

It is also important to underline recent research on this material, and in particular on web-crippling. Borowicz and Bank [7-9] focused on the IOF (Internal One Flange) loading of wide flange pultruded beams. And, more recently, Wu and Bai [10] have developed research in web-crippling on square hollow sections, in the ETF and ITF configurations.

Both Bank [16] and the Eurocomp [13], present similar design formulas for the web-crippling phenomenon. These expressions are based on the product between an effective resistant area and the ultimate transverse stress of the web. The design formulas presented by Bank [16] are displayed in (2)-(6),

$$F_{cr}^{crush} = (\sigma_y)_{cr}^{crush} A_{eff} \quad (2)$$

$$A_{eff} = t_w b_{eff} \quad (3)$$

$$h_w = h - 2t_f - 2R \quad (4)$$

$$b_{eff} = s_s + {}^{h_w}/_{2}, (ETF) \quad (5)$$

$$b_{eff} = s_s + h_w, (ITF) \quad (6)$$

where, F_{cr}^{crush} – crushing load; $(\sigma_y)_{cr}^{crush}$ – crushing stress; A_{eff} – effective area; s_s – bearing length; b_{eff} – effective length; h_w – web height; t_w – web thickness; t_f – flange thickness ; R – web-flange junction radius; h – beam depth.

These formulas have the benefit of being easy to apply, while differentiating end loading and interior loading conditions. The Eurocomp [13] presents a very similar formula, expressing the effective loaded length as the bearing length plus a 45º dispersion through half the web's height [13].

Both these references also share their approach on the web-buckling issue, by considering a different formula for this failure mode. These alternative formulas also share their starting point: considering the web as a simply supported plate. These formulas do not adopt any strength parameter of the material as they simply give elastic critical loads. Bank's web-buckling formula is presented in (7) and (8).

$$F_{cr} = \sigma_y^{cr} A_{eff} \quad (7)$$

$$\sigma_y^{cr} = \frac{2\pi^2}{t_w b_{eff}^2} (\sqrt{D_L D_T} + D_{LT} + 2\, D_S) \quad (8)$$

where: D_L, D_T, D_{LT} e D_S – plate properties; t_w – web thickness; b_{eff} – effective length (5) and (6); A_{eff} – effective area (3).

The Eurocomp [13] presents a similar design formula, which can be analyzed in (9)-(12),

$$\sigma_{cr} = \frac{k\pi^2 \sqrt{D_x D_y}}{{b_{eff}}^2 t_w} \quad (9)$$

$$b_{eff} = (h^2 + {S_s}^2)^{0,5} \quad (10)$$

$$k = 2\left(1 + \frac{H_0}{\sqrt{D_x D_y}}\right) \quad (11)$$

$$H_0 = 0{,}5(\nu_{xy} D_y + \nu_{yx} D_x) + \frac{(G t_w^3)}{6} \quad (12)$$

where: σ_{cr} – critical buckling stress; D_x, D_y – plate properties; h – beam depth; t_w – web thickness; S_s – bearing length; υ_{xy} –longitudinal Poisson coefficient; υ_{yx} – transverse Poisson coefficient; G – elastic shear modulus.

More recently, Wu and Bai [10] performed web-crippling tests on GFRP square hollowed sections and developed a new design expression on the basis of their experimental results. The expression presented by these authors follows that proposed by Borowicz and Bank [8], as it considers the interlaminar shear strength as the key resistance parameter, instead of the web transverse stress. Their expressions are given by

$$A_{shear} = 2t_w b_{plate} / \cos(45º)\, (2\, webs) \quad (13)$$

$$R_N = a_e f_s A_{shear}, (ETF) \quad (14)$$

$$R_N = a_i f_s A_{shear}, (ITF) \quad (15)$$

where: A_{shear} – shear area; t_w – web thickness; b_{plate} – bearing length; R_N –web crippling capacity; a_e – ETF coefficient (recommended value of 0,58); a_i – ITF coefficient (recommended value of 1,07); f_s – interlaminar shear strength.

Wu and Bai [10] also tested the formula presented by Borowicz and Bank [8] for the IOF configuration and compared it to their test results. They concluded that the expression proposed by Borowicz and Bank showed poor accuracy, when applied to the ETF and ITF configurations.

The formulae presented in (14)-(15) require the knowledge of the interlaminar shear strength, which was not known for both the I120 and I400 beams. In order to apply these design expressions to both these beams, the in-plane shear strength was considered instead, as an approximation.

4.2 - Comparison between design and experimental results

An assessment into the validity of two design formulas concerning web-crippling is presented in this section. The formula presented by Bank [16] and the expression presented by Wu and Bai [10] were compared to the experimental results. This comparison is presented in Table 5.

From the results presented in Table 5, it is easily concluded that Bank´s formula [16] doesn´t fit the experimental results, and that the formula developed by Wu and Bai [10] cannot be directly applied to I-shaped beams (the only calibration considered was made in equation (13), by considering half the effective shear area). For a more extensive analysis of the various design formulae see [11].

4.3 - Proposed design equation

On the basis of previously presented expressions, it would be rather important to develop new and accurate design formulae. Thus, analytical expressions based on the design formulae presented by the American Iron and Steel Institute for cold-formed steel sections [17] were developed. The European code EC3: 1-5 [18] was also taken into account, by providing a basis for a buckling reduction factor. The American design formula (16) has the advantage of being easily calibrated, because it consists in consecutive products of non dimensional ratios.

$$P_n = C\, t_w^2\, F_y \left(1 - C_R\sqrt{\frac{R}{t_w}}\right)\left(1 + C_N\sqrt{\frac{N}{t_w}}\right)\left(1 - C_h\sqrt{\frac{h_w}{t_w}}\right) \qquad (16)$$

where: C, C_R, C_N, C_h – empirical coefficients; h_w – web height; t_w – web thickness; F_y – steel yield stress; R – web-flange junction radius; N – bearing length; P_n – web crippling capacity.

The EC3: 1-5 [18] formulas are presented in (17)-(22).

$$\chi_F = \frac{0{,}5}{\bar{\lambda}_F} \qquad (17)$$

$$\bar{\lambda}_F = \sqrt{\frac{l_y\, t_w\, f_{yw}}{F_{cr}}} \qquad (18)$$

$$F_{cr} = 0{,}9\, k_f\, E\, \frac{t_w^3}{h_w} \qquad (19)$$

$$l_y = s_s + 2\, t_f\, (1 + \sqrt{m_1 + m_2}) \qquad (20)$$

$$m_1 = \frac{f_{yf}\, b_f}{f_{yw}\, t_w} \qquad (21)$$

$$m_2 = 0{,}02\left(\frac{h_w}{t_f}\right)^2, \quad for\ \bar{\lambda}_F > 0{,}5; \qquad m_2 = 0, \quad for\ \bar{\lambda}_F < 0{,}5 \qquad (22)$$

Table 5: Comparison between design and experimental results.

Beam	Bear. Length (mm)	ETF					ITF				
		Exp. (kN)	Bank (kN)	Ratio	Wu and Bai (kN)	Ratio	Exp. (kN)	Bank (kN)	Ratio	Wu and Bai (kN)	Ratio
I100	15	16,77	32,19	1,92	3,28	0,20	29,81	55,61	1,87	6,05	0,20
	50	33,00*	52,68	1,60	10,94	0,29	41,11	76,10	1,85	20,17	0,49
	100	45,48	81,95	1,80	21,87	0,48	56,50	105,36	1,86	40,35	0,71
I120	15	19,66	44,65	2,27	2,27	0,12	32,17	78,41	2,44	4,19	0,13
	50	38,88	70,06	1,80	7,58	0,19	51,96	103,82	2,00	13,98	0,27
	100	64,86	106,36	1,64	15,16	0,23	76,97	140,12	1,82	27,96	0,36
I200	15	37,15	87,93	2,37	3,63	0,10	67,83	161,98	2,39	6,69	0,10
	50	78,17	120,33	1,54	12,09	0,15	110,92	194,38	1,75	22,30	0,20
	100	115,33	166,61	1,44	24,17	0,21	161,34	240,66	1,49	44,59	0,28
I400	100	73,99	290,52	-	25,84	0,35	127,26	475,40	-	47,67	0,37

*Average value corrected due to the strange behavior of test specimen I100-ETF-50-2.

where: f_{yw} – web yield stress; f_{yf} – flange yield stress; l_y – effective length of bearing; χ_f – reduction factor, related to buckling phenomena; E – elastic modulus of the web; b_f – flange width; t_f – flange thickness; h_w – web height; t_w – web thickness; s_s – bearing length; k_f – coefficient related to the load configuration [18].

Based on expressions (16)-(22) a new empirical design formula was calibrated (23). The empirical coefficients determined for the ETF and ITF configurations are presented in Table 6. These coefficients were obtained through multiple regression, by minimizing the error for each experimental series, and considering different values for the ETF and ITF configurations. The main calibrations considered, in order to apply steel design formulas to GFRP beams, consisted in replacing the steel yield stress with the web transverse critical stress of the GFRP beam, and replacing the steel elastic modulus with the elastic transverse modulus of the GFRP profile. On the other hand, "R" was considered as the sum of the corner radius (of the web-flange junction) and the flange thickness.

The main principle in the creation of equation (23) is giving greater relevance to the bearing length, as well as further diminishing the resistance of a beam, based on its slenderness. The variables in expression (23) are the same as in expressions (16)-(22), with the exception of "C_χ", which is an empirical coefficient that multiplies the buckling ratio.

The results obtained through formula (23) are compared to the experimental results in Figs. 12 and 13. The results concerning the I100, I120 and I200 beams are very consistent, as they are supported by three separate lengths of bearing. The I400 beam was only tested with one length of bearing (100 mm) and thus, cannot be validated for other lengths of bearing. The design formula developed will certainly need future calibrations, and should be further tested with other cross-section shapes. One key issue is the influence of elastic buckling on web-crippling failure. This study will certainly allow for a better determination of the reduction factor on the basis of beam slenderness.

Table 6: Empirical coefficients for expression (23).

ETF			
C	C_R	C_{Nh}	C_χ
0,0688	0,5757	0,0037	0,0647
ITF			
C	C_R	C_{Nh}	C_χ
0,1489	0,5492	0,0015	0,0634

$$P_n = C * fy * {h_w}^2 * \left(1 - C_R * \sqrt{\frac{R}{t_w}}\right) * \left(1 + C_{Nh} * \frac{{h_w}^2 * N}{{t_w}^3}\right) * \left(1 - C_\chi * \frac{h_w}{t_w} * (1 - \chi_f)\right) \quad (23)$$

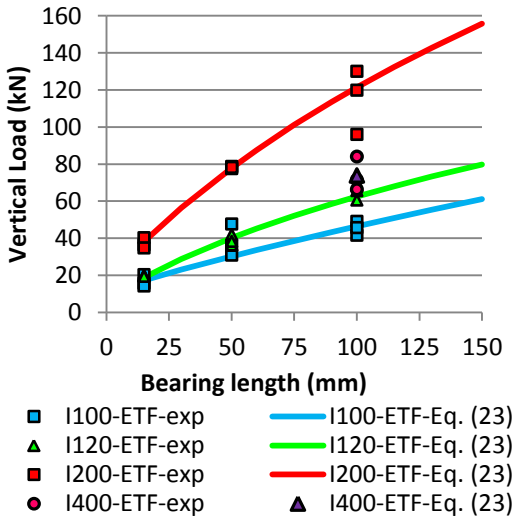

Fig. 12: Comparison between experimental and design results for the ETF configuration.

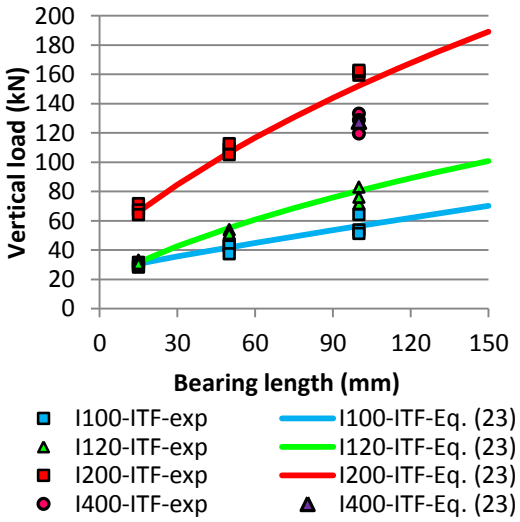

Fig. 13: Comparison between experimental and design results for the ITF configuration.

5 - Conclusions

The comprehensive research summarized in this paper provided several findings, at the various levels of the research conducted.

The experimental campaign highlighted the great importance of the bearing length on the web-crippling of GFRP beams. In fact, increasing the bearing length a few centimeters (1,5 to 10 cm) provided load capacity increases over 100 % for the majority of the profiles. The specimens tested in the ITF configuration presented the highest values of resistance and stiffness; while those tested in the ETF configuration presented the highest increase of mechanical performance with the bearing length. Furthermore, the increase of the bearing length also mitigated the local crushing of the web under the bearing plates, causing a more linear load-displacement behavior. The mechanical characterization campaign provided most of the required values for the numerical simulation and design formulae evaluation. However, it pointed out an important issue for future research: the need for an accurate determination of the elastic modulus in compression, a very important parameter for numerical simulation and for the study of web-buckling phenomena.

The numerical simulation allowed the assessment of the Tsai-Hill criterion, which proved to be excessively conservative; and the assessment of stress distributions, regarding different bearing lengths. In particular, the numerical models identified the edges of the bearing plates as critical areas, presenting considerable stress concentrations. The numerical simulation was also useful in validating the material's mechanical characterization and the failure mode analysis.

Finally, the main formulae, concerning web-crippling and web-buckling failure in GFRP beams were studied and compared with the experimental results, showing poor efficacy. Therefore, a new empirical design formula was developed, based on design formulae developed for steel elements. The results provided by this formula were consistent and in good agreement with the experimental data.

References

[1] Correia J.R., Branco F.A., Silva N.M.F., Camotim D. and Silvestre N., "First-order, buckling and post-buckling behaviour of GFRP pultruded beams. Part 1: Experimental study", Computers and Structures, Vol. 89, No. 21-22, pp. 2052-2064, 2011.

[2] Silva N.M.F., Camotim D., Silvestre N., Correia J.R., Branco F.A., "First-order, buckling and post-buckling behaviour of GFRP pultruded beams. Part 2: Numerical simulation", Computers and Structures, Vol. 89, No. 21-22, pp. 2065-2078, 2011.

[3] Correia J. R., Branco F. A. and Ferreira J. G., "The effect of different passive fire protection systems on the fire reaction properties of GFRP pultruded profiles for civil construction", Composites Part A: Applied Science and Manufacturing, Vol. 41, No. 3, pp. 441-452, 2010.

[4] Correia M., "Structural behaviour of GFRP pultruded profiles", Master Dissertation, Instituto Superior Técnico, Lisbon, 2012. *(in Portuguese)*

[5] Nunes F., "Structural behaviour of GFRP pultruded profiles strengthened with CFRP mats", Master Dissertation, Instituto Superior Técnico, Lisboa, 2012. *(in Portuguese)*

[6] Nunes F., Correia M., Correia J.R., Silvestre N. and Moreira A., "Experimental and numerical study on the structural behavior of eccentrically loaded GFRP columns", Thin-Walled Structures, Vol. 72, pp. 175-187, 2013.

[7] Borowicz D. T. and Bank L. C., "Behaviour of Pultruded Fiber-Reinforced Polymer (FRP) Beams Subjected to Concentrated Loads in the Plane of the Web", Second official International Conference of International Institute for FRP in Construction for Asia-Pacific Region, pp. 13-18, Seoul, 2009.

[8] Borowicz D. T. and Bank L. C., "Behaviour of Pultruded Fiber-Reinforced Polymer Beams Subjected to Concentrated Loads in the Plane of the Web", Journal of Composites for Construction, Vol. 15, No. 2, pp. 229-238, 2011.

[9] Borowicz D. T. and Bank L. C., "Effect of web reinforcement on the behavior of pultruded fiber-reinforced polymer beams subjected to concentrated loads", Construction and Building Materials, Vol. 47, pp. 347-357, 2013.

[10] Wu C. and Bai Y., "Web crippling behaviour of pultruded glass fibre reinforced polymer sections", Composite Structures, Vol. 108, pp. 789-800, 2014.

[11] Almeida Fernandes L., "Structural behaviour of GFRP beams subjected to concentrated loads: experimental tests, numerical modelling and analytical study", Master Dissertation in Civil Engineering, Instituto Superior Técnico, Lisbon, 2014. *(in Portuguese)*

[12] Simulia, "Abaqus/CAE", version 6.10, 2010.

[13] Eurocomp, "Structural Design of Polymer Composites", the European Structural Polymeric Composites Group (Editor: J. L. Clarke), E & Fn Spon, London, 1996.

[14] CNR-DT 205/2007, "Guide for the Design and Construction of Structures made of FRP Pultruded Elements", National Research Council of Italy, Rome, 2008.

[15] "Pre-Standard for Load & Resistance Factor Design (LRFD) of Pultruded Fiber Reinforced Polymer Structures (FRP)", American Society of Civil Engineers (ASCE), 2010.

[16] Bank L. C., "Composites for Construction: Structural Design with FRP materials", Wiley, Hoboken, 2006.

[17] AISI S100-2007, "North American Cold-Formed Steel Specification", American Iron and Steel Institute (AISI), Washington D.C., 2007.

[18] EN 1993-1-5:2004, "Eurocode 3 – Part 1-5: Plated Structural elements", European Committee for Standardization (CEN), draft 49, Brussels, 2004.